Applied Thermal Engineering 256 (2024) 124137

Contents lists available at ScienceDirect

Applied Thermal Engineering

journal homepage: www.elsevier.com/locate/apthermeng

Research Paper

Gaussian process regression to predict dryout incipience quality of saturated flow boiling in mini/micro-channels

Arshad Afzal [a], Seunghyun Lee [a,*], Sung-Min Kim [b], Issam Mudawar [c]

[a] Two-Phase Flow and Thermal Management Laboratory, School of Mechanical Engineering, Gwangju Institute of Science and Technology, 123 Cheomdangwagi-ro, Buk-gu, Gwangju 61005, South Korea
[b] School of Mechanical Engineering, Sungkyunkwan University, 300 Cheoncheon-dong, Suwon 16419, South Korea
[c] Purdue University Boiling and Two-Phase Flow Laboratory (PU-BTPFL), School of Mechanical Engineering, 585 Purdue Mall, West Lafayette, IN 47907, USA

ARTICLE INFO

Keywords:
Mini/micro-channels
Heat transfer coefficient
Saturated flow boiling
Dryout incipience
Machine learning
Gaussian process regression

ABSTRACT

In the present study, a Gaussian process regression (GPR) model is developed to predict the dryout incipience quality for flow boiling in mini / micro – channels based on a consolidated database obtained from Purdue University Boiling and Two – Phase Flow Laboratory (PU – BTPFL) consisting of 997 points from 26 sources. The database includes 13 different working fluids over a wide range of operating conditions: hydraulic diameter (0.51 – 6.0 mm), mass velocities (29 – 2303 kg/ m^2 s), liquid – only Reynolds number (125 – 53,770), boiling number (0.31 – 44.3 × 10^{-4}), and reduced pressure (0.005 – 0.78). The inputs to the model were liquid – only Weber number (We_{fo}), reduced pressure (P_R), boiling number (Bo), heated to frictional perimeter ratio(P_H/P_F), capillary number (Ca) and density ratio (ρ_g/ρ_f), and the output was dryout incipience quality. The database was randomly divided into training data to learn GPR kernel (covariance) parameters using maximum likelihood estimation, and test data to evaluate the prediction accuracy of the outputs based on mean absolute error (MAE). Six – different types of covariance functions were tested, and GPR model with automatic relevance detection (ARD) rational quadratic covariance function showed the best overall performance. A performance comparison of approved GPR model was made with an existing highly reliable universal correlation to predict dryout incipience quality for mini / micro – channels. Results show that the developed GPR model exhibits superior generalization ability with an overall MAE of 6.03 %, and a significant reduction of 51.76 % in MAE compared with the universal correlation. Overall, the GPR model was found to be a data efficient machine learning technique for predicting dryout incipience quality for flow boiling in mini / micro – channels based on a consolidated database.

1. Introduction

Efforts towards miniaturization and seamless integration in contemporary technology have ushered in the era of ultra-high heat flux devices [1]. Effectively dissipating a substantial amount of heat from a small surface has emerged as a paramount concern. This technological trajectory has heightened the significance of thermal management for these devices, as maintaining them within the optimal temperature range is a critical prerequisite for achieving their designed performance. Among the myriad thermal management methods, the cooling technique employing two-phase flow boiling has garnered considerable attention as a robust contender for addressing the thermal challenges posed by ultra-high heat flux devices [2]. Its superior cooling performance stems from a heat transfer mechanism that leverages both sensible and latent heats [3]. To optimize cooling efficiency, the flow boiling technique has been implemented in micro-channels, showcasing a high heat transfer coefficient for single-phase convection [2,4 –6]. Micro-channel flow boiling has been integrated into diverse cooling techniques, encompassing parallel micro-channel heat sinks [7 –10], manifold micro-channel heat sinks [11], hybrid cooling involving jet impinging on micro-channels [12], and capillary-driven evaporator [13], and buoyancy-driven pumpless loops [14]. These applications span various devices, including power semiconductors [15,16], avionics [17], batteries [18], HVAC (heating, ventilation, and air-conditioning) systems [19], nuclear reactors [20], rocket nozzles [21], and hydrogen stacks [22,23]. Characterized by a high heat transfer rate at a given temperature difference, the mentioned cooling techniques offer advantages such

* Corresponding author.
E-mail address: lees@gist.ac.kr (S. Lee).

https://doi.org/10.1016/j.applthermaleng.2024.124137
Received 13 April 2024; Received in revised form 21 June 2024; Accepted 6 August 2024
Available online 11 August 2024
1359-4311/© 2024 Elsevier Ltd. All rights are reserved, including those for text and data mining, AI training, and similar technologies.

Nomenclature

A	flow area
A_{ch}	channel cross-sectional area
Bo	boiling number,q''_H/Gh_{fg}
Ca	capillary number,$\mu_f G/(\rho_f \sigma)$
D	diameter; terms used in Eq. (12) for loss function
D_h	hydraulic diameter
Fr	Froude number,$G^2/\rho^2 g D_h$
f	frictional factor
h_{tp}	two-phase heat transfer coefficient
h_{fg}	latent heat of vaporization
i	index for i-th sample in database
n	number of data
P	pressure
P_{crit}	critical pressure
P_F	wetted perimeter of channel
P_H	heated perimeter of channel
P_R	reduced pressure, P/P_{crit}
q''	heat flux
q''_{CHF}	critical heat flux
q''_H	heat flux based on heated perimeter of channel
T	temperature
We	Weber number,$G^2 D_h/\rho\sigma$
x_{crit}	dryout completion (CHF) quality
x_{di}	dryout incipience quality
$x_{di}{}^*$	dryout incipience quality
$\boldsymbol{x}_i$	i^{th} sample input
y_i	i^{th} sample output

Acronyms

ARD	automatic relevance determination
CHF	critical heat flux
DNB	deviation from nucleate boiling
MAE	relative mean absolute error

Greek symbols

ε	error tolerance
θ	percentage predicted within in ±30%
μ	dynamic viscosity
ξ	percentage predicted within in ±50%
ρ	density
ρ_r	density ratio, ρ_g/ρ_f
σ	surface tension

Subscripts

crit	critical
ch	channel
di	dryout incipience
exp	experimental (measured)
f	saturated liquid
fo	liquid only
g	saturated vapor
go	vapor only
in	inlet
pred	predicted
r	ratio
sat	saturation
w	wall

as the ability to suppress temperature rise, maintain a uniform temperature along the flow direction, and minimize system size and weight. However, they also present drawbacks, including high pumping power [24], susceptibility to various flow instabilities [25–27], and the occurrence of premature critical heat flux (CHF) [28]. Particularly concerning flow instabilities and CHF, once they occur, they can lead to dryout and subsequent temperature rise in the downstream region, negating the mentioned thermal advantages. Given the paramount importance of operating temperature in modern devices, the occurrence of dryout is considered a pivotal event that demands precise prediction. Nevertheless, predicting dryout is a highly complex task due to the existence of multiple triggering mechanisms.

Dryout phenomena can be broadly categorized into two groups based on the associated phenomena they induce: premature critical heat flux (CHF) and CHF itself. Premature CHF, induced by severe vapor backflows, occurs when the liquid film is periodically evaporated in the downstream region, a phenomenon referred to as intermittent dryout [10,29,30]. These vapor backflows result from extensive phase changes and rapid bi-directional bubble expansion within the confined volume of the channel, accompanied by a high pressure drop along the mini/micro-channels [17,26,31]. These hydrodynamic instabilities manifest as severe pressure drop oscillations and mild parallel-channel instability [7]. CHF occurs when the vapor flow completely envelops the heated surface after the liquid film has undergone dryout or vapor film is generated in regions with relatively lower thermodynamic quality, respectively [3,32]. Liquid film dryout typically leads to a mild temperature rise in the downstream region, where mist flow, often accompanied by entrained liquid droplets, begins to appear following the annular flow regime. In contrast, vapor film generation, prevalent in subcooled or low-quality flows, results in rapid temperature rise, typically in the upstream region under high heat flux conditions, a phenomenon termed as deviation from nucleate boiling (DNB) CHF. Historically, predictive tools for dryout incipience quality focused on specific phenomena or operating conditions, rendering them unsuitable as general solutions for various situations [33–47]. Previous theoretical approaches attempted to model specific phenomena considered primary trigger mechanisms of dryout incipience, including premature annular film dryout by entrained liquid droplets [33–36], Kelvin-Helmholtz surface instability [37], and asymmetric liquid film establishment along the circumferential direction [38]. However, these theoretical models could describe only one of these mechanisms despite the potential for dryout initiation through various means. Empirical correlations from previous studies were developed using dimensionless numbers for flows with diverse geometries, operating conditions, fluids, and thermophysical properties [39–47]. Nonetheless, their predictive performance proved effective only for specific cases covered by the databases used to develop the correlations. In attempts to predict the complex dryout phenomena triggered by various factors, the majority of previous approaches have inherent limitations as general predictive tools due to their reliance on a limited range of data.

Kim and Mudawar [48] proposed a universal correlation based on a consolidated database of 997 points from 26 sources for a wide range of operating conditions and different types of working fluids, and showed a superior prediction accuracy compared to the previous correlations [39–47]. Over the last few decades, machine learning models such as neural networks, support vectors, and Gaussian processes have been widely used for predictive modeling in thermal – fluid applications [73–76]. One of the main advantage of machine learning models compared to empirical and semi – empirical correlations is its ability to automatically and efficiently capture the non – linearity in the output based on some specific types of basis – functions and algorithms with sufficient accuracy. Recently, Qiu et al. [75] used artificial neural networks (ANN) to predict heat transfer coefficient based on universal consolidated data for saturated flow boiling in mini / micro – channels. The ANN predictions

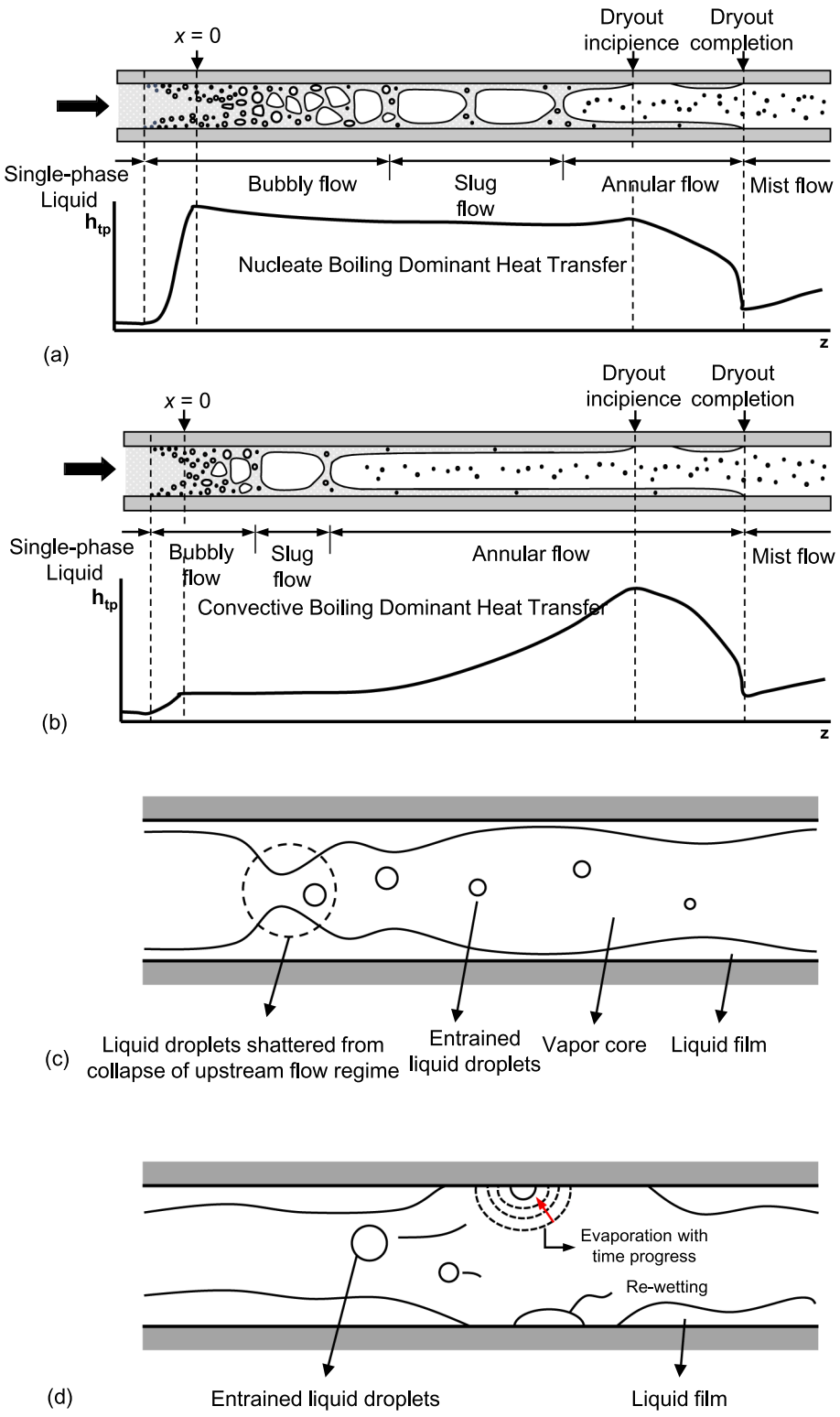

Fig. 1. Schematics of axial variation of flow regime and heat transfer coefficient along uniformly heated mini/micro-channel with downstream wall dryout for (a) nucleate boiling dominant heat transfer [48], (b) convective boiling dominant heat transfer [48], and detailed schematic depictions of (c) shattering [80] and (d) re-wetting by collision of entrained liquid droplets in partial dryout region.

were found to be superior to universal correlation, over combined as well as individual database, and offer advantage to test any combination of input parameters. Pearce et al. [76] used Gaussian process regression (GPR) for solving inverse problem to determine the parameters of a thermal model for gas turbine application. The GPR model was used to develop a surrogate for mean – squared error function that measures the discrepancy between simulation and experimental data. Afzal and Kim [77] performed optimization of pulsatile flow and geometry of a convergent – divergent micro-mixer using three different surrogate models, viz. response surface approximation, radial – basis neural networks and GPR models. The results indicated that the GPR model predicted the best optimum design among the tested models. In another

Table 1
Consolidated database for dryout incipience quality of saturated flow boiling in mini/micro-channel used to develop Gaussian process regression (GPR) model.

Author(s)	Channel Geometry	D_h[mm]	Fluid(s)	G[kg/ m^2s]	Data points	Remarks
Ali and Palm (2011) [55]	C, S, V	1.22, 1.70	R134a	50 – 600	23	x_{di} identified by change of slope in boiling curve, and wall temperature
Baek and Chang (1997) [58]	C, S, V	6.0	Water	29 – 277	232	x_{crit} indentified by fast increase of T_w when $T_w > 250$ °C
Becker (1970) [56]	C, S, V	2.4, 3.0	Water	365 – 2725	82	x_{crit} identified by fast increase of T_w
Del Col and Bortolin (2012) [70]	C, S, H	0.96	R134a, R245fa, R32	101 – 902	43	x_{di} identified by wall temperature
Ducoulombier et al. (2011) [39]	C, S, H	0.529	CO_2	200 – 1410	48	x_{di} identified by falling off of h_{tp}
Greco (2008) [65]	C, S, H	6.0	R134a, R22, R407C, R410A	199 – 1079	7	x_{di}* identified by falling off of h_{tp}
Hihara and Dang (2007) [64]	C, S, H	1.0, 2.0, 4.0, 6.0	CO_2	360 – 1440	16	x_{di} identified by falling off of h_{tp}
Karayiannis et al (2012) [71]	C, S, V	1.1	R134a	300	3	x_{di} identified by falling off of h_{tp}
Kim et al (2000) [60]	C, S, V	6.0	Water	99 – 277	210	x_{crit} identified by fast increase of T_w with T_w increase rate of 50 °C/s
Lezzi et al (1994) [57]	C, S, H	1.0	Water	776 – 2738	68	x_{crit} identified by fast increase of T_w when $T_w > 250$ °C
Li et al (2012) [54]	C, S, H	2.0	R1234yf, R32	100 – 400	8	x_{di}* identified by falling off of h_{tp}
Martin-Callizo (2010) [51]	C, S, V	0.64	R134a, R22, R245fa	185 – 541	42	x_{di} identified by change of slope in boiling curve, and wall temperature
Mastrullo et al (2012) [40]	C, S, H	6.0	CO_2, R410A	150 – 501	28	x_{di} identified by falling off of h_{tp}
Oh and Son (2011a) [52]	C, S, H	1.77, 3.36, 5.35	R134a, R22	200 – 400	6	x_{di}* identified by falling off of h_{tp}
Oh and Son (2011b) [68]	C, S, H	4.57	CO_2	600 – 900	8	x_{di}* identified by falling off of h_{tp}
Oh et al (2011) [69]	C, S, H	1.5, 3.0	R22, R410A, R290	100 – 500	9	x_{di}* identified by falling off of h_{tp}
Ohta et al (2009) [67]	C, S, H	0.51	FC72	107, 205	2	x_{di}* identified by falling off of h_{tp}
Roach et al (1999) [59]	C, S, H	1.168, 1.448	Water	256 – 1037	42	x_{crit} identified by fast increase of T_w when $T_w > 250$ °C
Saitoh et al (2005) [63]	C, S, H	0.51, 1.12, 3.1	R134a	150 – 300	41	x_{di}* identified by falling off of h_{tp}
Shiferaw (2008) [66]	C, S, H	1.1, 2.88, 4.26	R134a	200 – 400	13	x_{di}* identified by falling off of h_{tp}
Tibirica et al (2012) [72]	C, S, H	1.0	R1234ze	300 – 600	4	x_{di}* identified by falling off of h_{tp}
Wang et al (2009) [50]	C, S, H	1.3	R134a	321 – 676	9	x_{di}* identified by falling off of h_{tp}
Wu et al (2011) [53]	C, S, H	1.42	CO_2	300 – 600	18	x_{di}* identified by falling off of h_{tp}
Yang and Fujita (2002) [61]	R, S, H	0.976	R113	100, 200	3	x_{di}* identified by falling off of h_{tp}
Yu et al (2002) [62]	C, S, H	2.98	Water	50 – 151	30	x_{crit} identified by fast increase of T_w
Yun et al (2005) [49]	R, M,H	1.14	CO_2	300, 400	2	x_{di}* identified by falling off of h_{tp}
Total					997	

* R: rectangular, C: circular.
** S: single-channel, M: multi-channel.
*** H: horizontal-channel, V: vertical-channel.
**** x_{crit}: critical quality data reported by original authors.
***** x_{di}: dryout incipience quality data reported by original authors.
****** x_{di}*: dryout incipience quality data identified by other researchers by falling off in measured two-phase heat transfer coefficient attributed by original authors to dryout incipience.

study, optimization of staggered jet – convex dimple array cooling system was conducted using GPR model by Kim et al. [78] with a sufficiently high accuracy. Duan et al. [79] trained GPR models based on experimental measurements for making predictions at positions where there are no experimental data. The fitted model was then used to measure the discrepancy between experiment and computational fluid dynamics (CFD) simulation. ANNs are efficient, but require a very large dataset for training and testing to produce reliable and accurate results. On the other hand, Gaussian process regression (GPR) model offer the advantage of learning from data with small sample size, ability to capture noise (generally, white gaussian noise) in the experimental data based on its mathematical formulation.

It can be seen that GPR models have been used as a promising surrogate model for the analysis and optimization of wide range of thermal – fluid systems, but its predictive capabilities for applications involving complex systems needs to be analyzed. In the present study, a Gaussian process regression (GPR) model is developed to predict the dryout incipience quality for flow boiling in mini / micro – channels based on a consolidated database of 997 points from 26 sources [49 –72]. The working fluids and range of operating conditions are summarized below:

- Working fluid: FC72, R113, R1234yf, R1234ze, R134a, R22, R245fa, R290, R32, R407C, 410A, CO_2 and water.
- Hydraulic diameter: $0.51 < D_h < 6.0$ mm
- Mass velocity: $29 < G < 2303$ kg/ m^2s
- Liquid – only Reynolds number: $125 < Re_{fo} < 53,770$

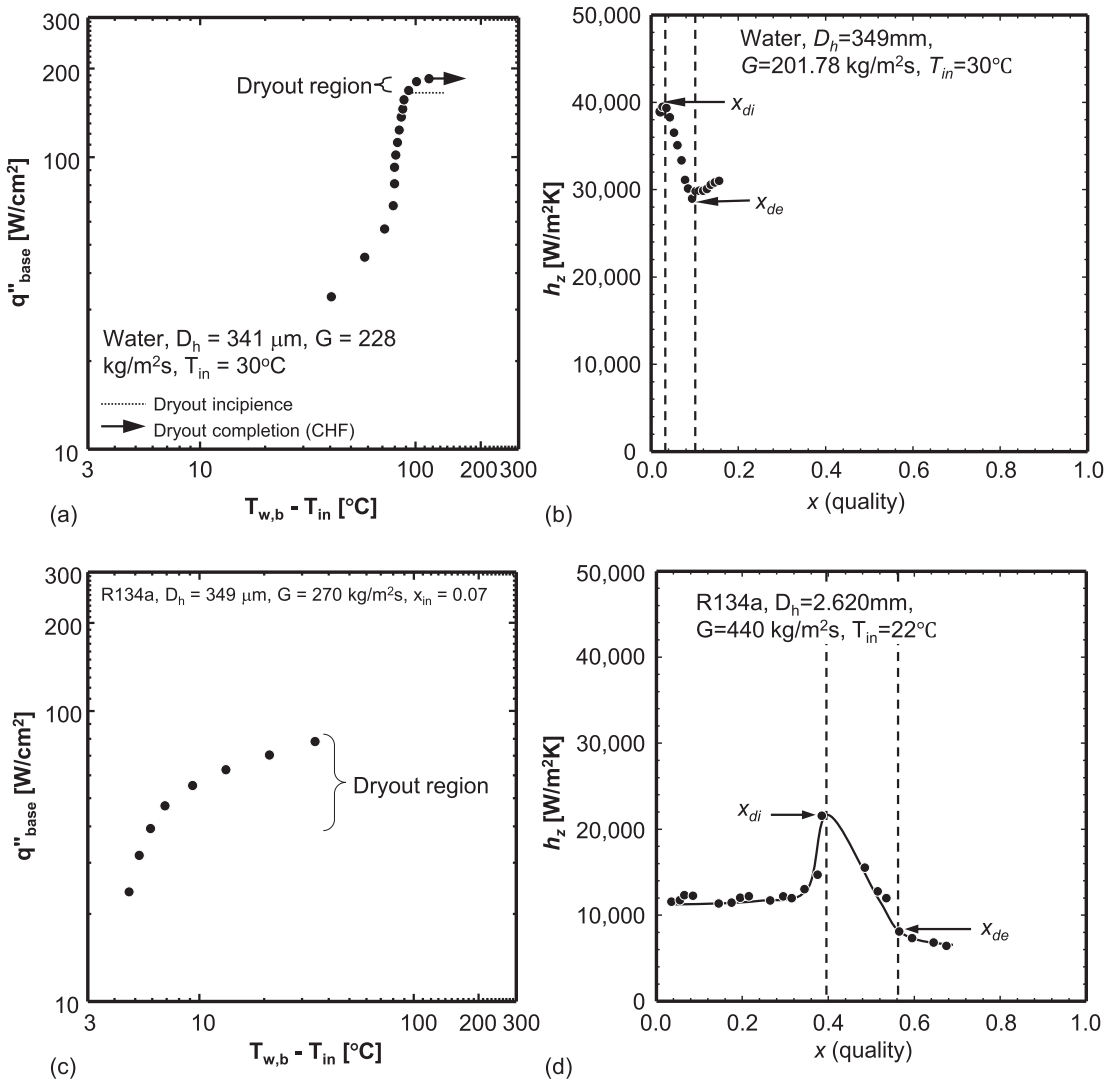

Fig. 2. Boiling curves and variation of local heat transfer coefficient with quality for (a) water [29] a nd (b) water [6], (c) R134a [8] and (d) R134a [81] flows in rectangular micro-channels.

– Boling number:.$0.31 \times 10^{-4} < Bo < 44.3 \times 10^{-4}$
– Reduced pressure:.$0.005 < P_R < 0.78$

The inputs parameters viz. liquid – only weber number (We_{fo}), reduced pressure (P_R), boiling number (Bo), heated to frictional perimeter ratio (P_H/P_F), capillary number (Ca) and density ratio (ρ_g/ρ_f), and the output, dryout incipience quality, were taken similar to Kim and Mudawar [48]. The predictive performance of the GPR model is compared with the universal correlation of Kim and Mudawar [48] using performance metrics, mean absolute error (MAE) and θ (percentage of predictions within ±30% of the data).

2. Mini / microchannel database

The hydrodynamic and thermal transport phenomena of flow boiling in micro-channels are complicated and affected by many unpredictable factors, but the general trends can be largely categorized into two: nucleate and convective boiling dominant heat transfer. While the axial transition pattern of the flow regime varies depending on the dominant heat transfer mechanisms, which are determined by the portion of the channel length occupied by either of them, as shown in Fig. 1(a) and 1 (b), the dryout incipience of saturated flow boiling in micro-channels occurs in the annular flow regime when the annular liquid film breaks. For nucleate boiling dominant heat transfer in Fig. 1(a), the bubbly flow regime occupies a large portion of the upstream channel length. The heat transfer is enhanced by the individual bubble motions in the bubbly flow regime, but it starts to decrease from the slug flow regime with suppressed bubble motions. In the annular flow regime, the asymmetric liquid film establishment causes partial breakage, allowing the heated wall to be exposed to vapor and decreasing the heat transfer coefficient. This point is termed dryout incipience, and the heat transfer coefficient steadily decreases until the liquid film is completely evaporated, considered as dryout completion. For convective boiling dominant heat transfer in Fig. 1(b), the annular flow regime, which is initiated farther upstream compared to nucleate boiling, occupies the largest portion of the channel length. Conduction through the liquid film is the dominant heat transfer mechanism, and the heat transfer coefficient increases in an axial direction as the liquid film becomes thinner due to interfacial evaporation. The partial annular film breakage in the following downstream region can be triggered by non-uniform evaporation or other factors that break the symmetry of the annular liquid film. Among these explanations, one possibility is that entrained liquid droplets generated by shattering can cause partial liquid film breakages, as illustrated in Fig. 1(c) [80]. When deposited on the heated surface, these entrained liquid droplets, together with the partial liquid film, can facilitate partial heat transfer and prevent CHF occurrence, as shown in

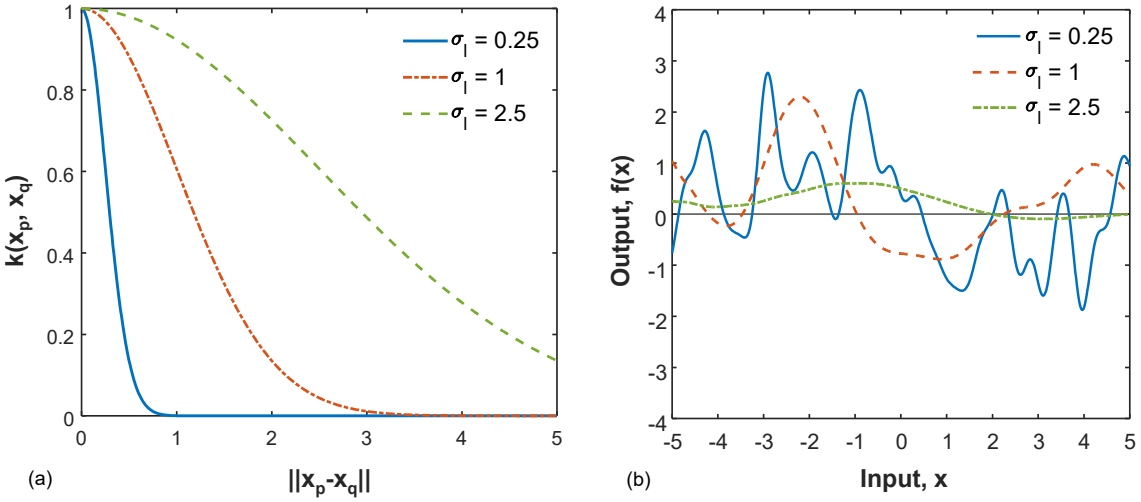

Fig. 3. (a) covariance functions and (b) random functions drawn from the Gaussian processes with squared exponential covariance function for different values of characteristic length parameter, σ_1.

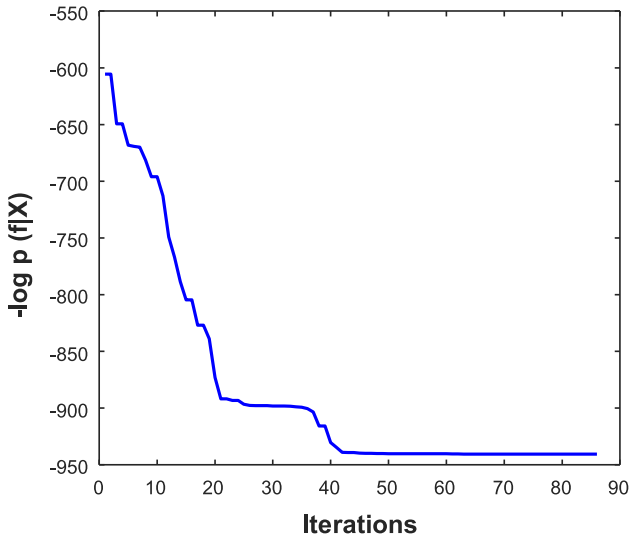

Fig. 4. Marginal log likelihood function versus number of iterations for ARD rational quadratic kernel.

Fig. 1(d).

The detailed consolidated database for dryout incipience quality of saturated flow boiling in mini/micro – channels for different working fluids and range of operating conditions is provided in Table 1. The consolidated database consisting of 997 dryout incipience qualities amassed from 26 sources is divided into three types, x_{crit}, x_{di}, and, x^*_{di} according to how they are identified. The first type is x_{crit} which corresponds to the dryout completion point where the liquid film completely dries out and partial cooling is conducted by collision of liquid droplets entrained in mist flows as shown in Fig. 1(a) and 1(b), where the sudden wall temperature rise from the saturation temperature is observed with heat transfer coefficients maintained low values [56–60,62]. The dryout completion is one of three types of critical heat flux (CHF): subcooled departure from nucleate boiling (DNB), saturated DNB and complete dryout, and this is the reason we termed it CHF (dryout completion) quality, x_{crit}. Apparently, x_{crit} is different from x_{di} which occurs by the partial liquid film breakage causing relatively smaller temperature rise as shown in Fig. 1(d). However, these two, especially for water, have similar values as the dryout completion follows dryout incipience just right after its occurrence which is evidenced by the sharp transition from x_{di} to x_{crit} that is shown at the wall temperature slightly higher than the saturation temperature in boiling curve as depicted in Fig. 2(a) [29]. A variation of heat transfer coefficient depicted in Fig. 2(b) also clearly shows this sharp transition, which convinces to use x_{crit} as x_{di} [6]. The water, with high surface tension, has relatively small amount of entrained liquid droplets attributing to stable two-phase interface maintaining high resistance to shattering, and this is the reason for sudden heat transfer coefficient drop without liquid droplet collision effect [6]. The drastic temperature excursion at CHF is caused by superior thermophysical properties of water that enables maintaining relatively high heat transfer coefficient while the dryout is in process before dryout completion (CHF). Combined with complicated flow physics under instability, the dryout completion (CHF) in mini/microchannel necessitates further researches to elucidate detailed trigger mechanisms. 664 x_{crit} data points are amassed from 6 sources those are all water and identified by temperature rise from T_{sat} by 5 to 150 °C [56–60,62]. 333 data points, denoted as x_{di}, were collected from 20 sources, primarily composed of fluids other than water. These data points exhibited a gradual slope change in the boiling curve, indicating a broad dryout range with partial dryout behavior, as shown in Fig. 2(c). This

Table 2
Maximum likelihood estimate of the hyperparameters of the different covariance functions and noise

Covariance Function	Hyperparameters	
	$\theta = [\sigma_l \quad \alpha \quad \sigma_f]$	σ_n
Exponential	[97.10 – 0.53]	0.10
Squared Exponential	[627.88 – 0.41]	0.13
ARD Exponential	[397.65 0.60 8.26×10^{-3} 0.03 0.02 46.19 0.54 –]	0.01
ARD Squared Exponential	[580.94 0.14 3.76×10^{-4} 0.03 0.02 0.14 0.55 –]	0.08
Rational Quadratic	[627.92 0.01 0.53]	0.12
ARD Rational Quadratic	[4.81 0.01 1.86×10^{-4} 4460 3.28×10^{-4} 1.38 3.50×10^{-3} 0.62]	0.01

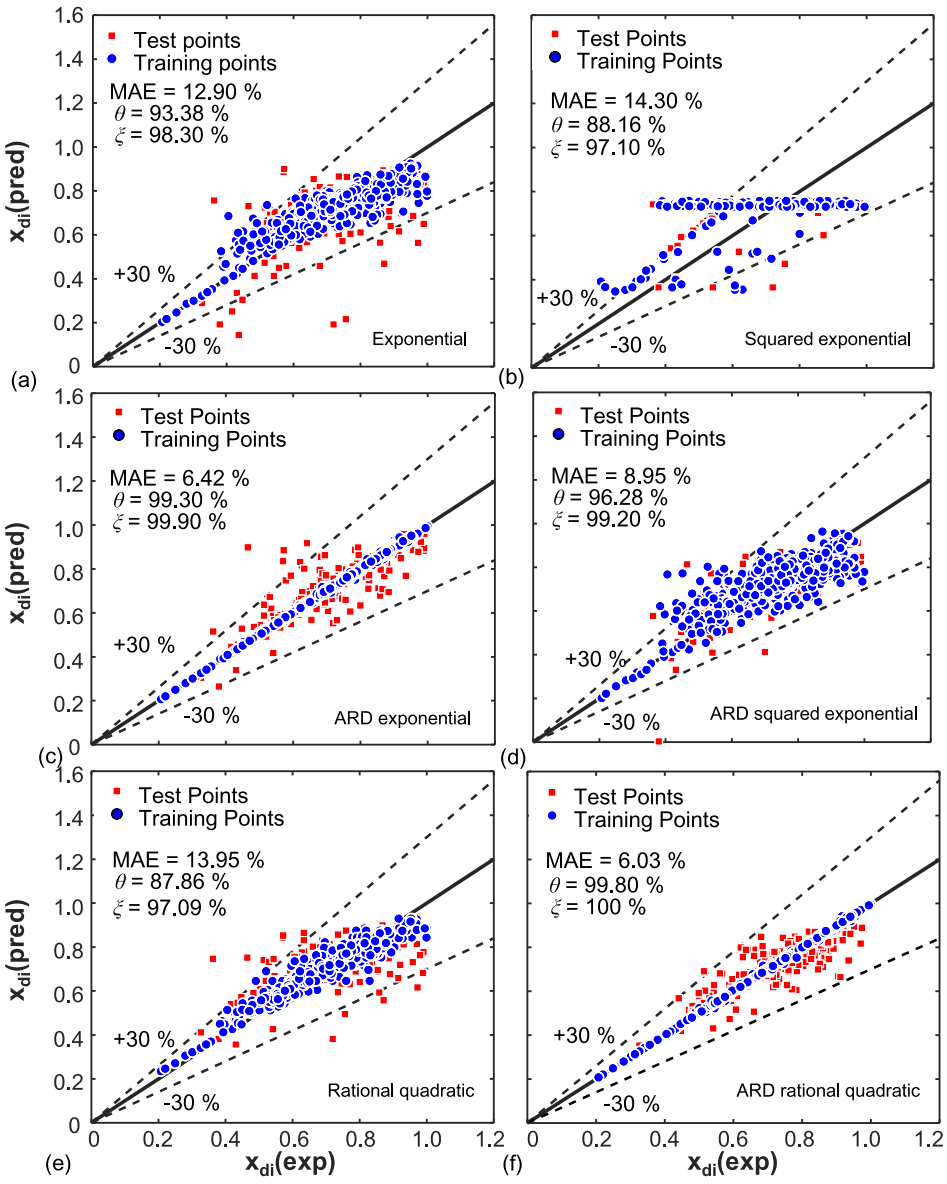

Fig. 5. Predictions from the GPR model for different covariance functions: (a) exponential, (b) squared exponential, (c) ARD exponential, (d) ARD squared exponential, (e) rational quadratic and (f) ARD rational quadratic.

behavior differs from the observed pattern in 664 x_{crit} data points. The inferior thermophysical properties and relatively low Critical Heat Flux (CHF) compared to water are attributed to this gradual transition from dryout incipience to completion. This dataset is further divided into two subsets: x_{di} and x^{*}_{di}. The former, x_{di}, was identified by previous researchers through mild temperature rise [39,40,51,55,64,70,71], while the latter,x^{*}_{di}, was identified based on the quality at which the heat transfer coefficient begins to decrease [49,50,52–54,61,63,65–69,72].

3. Gaussian process regression (GPR)

A Gaussian process is a collection of random variables, such that any finite number of those variables have a joint Gaussian distribution [82]. For regression, the random variable represents the value of the function, $f(\boldsymbol{x})$ at location, $\boldsymbol{x}$. A Gaussian process is completely specified by its mean function and a covariance function. The mean and the covariance function, $\mu(\boldsymbol{x})$ and $k(\boldsymbol{x},\boldsymbol{x}')$ of a real process $f(\boldsymbol{x})$ are defined as:

$$\mu(\boldsymbol{x}) = \mathrm{E}[f(\boldsymbol{x})] \tag{1}$$

and

$$k(x,x') = \mathrm{E}[(f(x)-\mu(x))(f(x')-\mu(x'))] \tag{2}$$

and the Gaussian process is written as:

$$f(\boldsymbol{x}) \sim \mathrm{GP}(\mu(\boldsymbol{x}), k(\boldsymbol{x},\boldsymbol{x}')) \tag{3}$$

The mean function, $\mu(\boldsymbol{x})$, represents the trend over the design space, and the covariance function captures the smoothness of the response. The covariance function specifies the covariance between pair of random variables:

$$\mathrm{cov}(f(\boldsymbol{x}_p), f(\boldsymbol{x}_q)) = k(\boldsymbol{x}_p, \boldsymbol{x}_q) \tag{4}$$

where $\boldsymbol{x}_p, \boldsymbol{x}_q \in \mathbb{R}^{\boldsymbol{d}}$. In other words, it determines the similarity between the data points $\boldsymbol{x}_p$ and $\boldsymbol{x}_q$; a basic assumption that if points $\boldsymbol{x}_p$ and $\boldsymbol{x}_q$ are close their response points y_p and y_q are also similar. Thus, training points that are near to a test point should be informative about the prediction at that point. The different types of covariance functions, and their mathematical forms are summarized below:

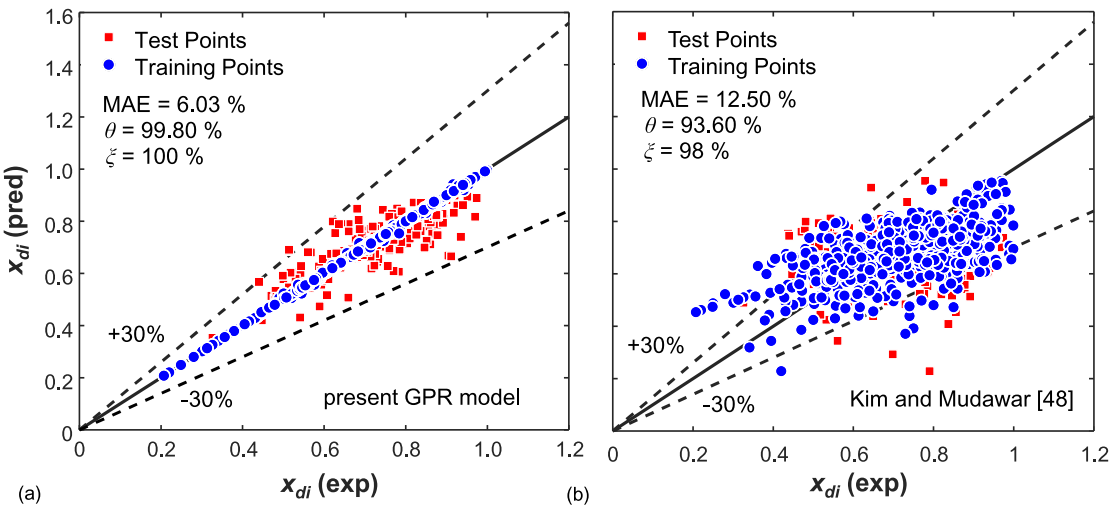

Fig. 6. Comparison of predictions from (a) approved GPR model and (b) universal correlation of Kim and Mudawar [48] for consolidated 997 point database.

1. Exponential covariance function

$$k(x_p, x_q) = \sigma_f^2 \exp\left[-\frac{\|(x_p - x_q)\|}{\sigma_l}\right] \tag{5}$$

2. Squared exponential covariance function

$$k(x_p, x_q) = \sigma_f^2 \exp\left[-\frac{1}{2}\frac{\|(x_p - x_q)\|^2}{\sigma_l^2}\right] \tag{6}$$

3. ARD exponential covariance function

$$k(x_p, x_q) = \sigma_f^2 \exp\left[\sum_{m=1}^{d}\frac{\|(x_{pd} - x_{qd})\|^2}{\sigma_m^2}\right]^{\frac{1}{2}} \tag{7}$$

4. ARD squared exponential covariance function

$$k(x_p, x_q) = \sigma_f^2 \exp\left[-\frac{1}{2}\sum_{m=1}^{d}\frac{\|(x_{pd} - x_{qd})\|^2}{\sigma_m^2}\right] \tag{8}$$

5. Rational quadratic covariance function

$$k(x_p, x_q) = \sigma_f^2\left(1 + \frac{\|(x_p - x_q)\|^2}{2\alpha\sigma_l^2}\right)^{-\alpha} \tag{9}$$

6. ARD rational quadratic covariance function

$$k(x_p, x_q) = \sigma_f^2\left(1 + \frac{1}{2\alpha}\sum_{m=1}^{d}\frac{\|(x_{pd} - x_{qd})\|^2}{2\alpha\sigma_d^2}\right)^{-\alpha} \tag{10}$$

For the exponential, squared exponential and rational quadratic covariance functions, σ_f is the signal standard deviation,σ_l is characteristic length scale and α is the positive – valued scale – mixture parameter. However, $\boldsymbol{\sigma}_l \in \mathbb{R}^{\boldsymbol{d}}$ is a vector with a separate length scale for each predictor for the class of ARD covariance functions. In practice, all covariance function parameters are grouped under a single vector parameter, $\boldsymbol{\theta}$. The form of the squared exponential covariance function, and samples drawn from it for different values of the characteristic length parameter, $\sigma_l = 0.25, 1, 2.5$ are illustrated in Fig. 3. It can be seen that low values of σ_l leads to sharp variations in the underlying function, whereas high values of σ_l can be used to capture a slowly varying function.

Given a set of n training data points, $\{(\boldsymbol{x_i}, y_i), i = 1, 2, \cdots, n\}$, where $\boldsymbol{x_i} \in \mathbb{R}^{\boldsymbol{d}}$ and $y_i \in \mathbb{R}$, a Gaussian process regression (GPR) model aims to predict the value of a response variable, y_* given the new input vector, $\boldsymbol{x}_* \in \mathbb{R}^{\boldsymbol{d}}$. In realistic modeling situations, there is always some noise present in the data, and therefore the problem becomes:

$$y = f(x) + \in \tag{11}$$

where $\in N(0, \sigma_n^2)$ is an additive independent identically distributed Gaussian noise with noise variance, σ_n^2. The covariance function is modified to incorporate noise, and is expressed as:

$$\mathrm{cov}\left(y_p, y_q\right) = k(x_p, x_q) + \sigma_n^2\delta_{pq} \tag{12}$$

where δ_{pq} is a Kronecker delta which is equal to 1 if $p = q$, and 0 otherwise. The joint distribution of the observed training outputs, and the test outputs according to the prior is:

$$\begin{bmatrix} y \\ f^* \end{bmatrix} \sim N\left(0, \begin{bmatrix} \mathrm{K(X, X)} + \sigma_n^2 & \mathrm{K(X, X_*)} \\ \mathrm{K(X_*, X)} & \mathrm{K(X_*, X_*)} \end{bmatrix}\right) \tag{13}$$

If there are n training points, then $\mathrm{K(X, X_*)}$ denotes the $n \times 1$ matrix of the covariances evaluated at all pairs of training and test points, $\mathrm{K(X,\ X)}$ denotes the $n \times n_*$ matrix at all pair of training points, and similarly for $\mathrm{K(X_*,\ X_*)}$, and $\mathrm{K(X_*,\ X)}$. By conditioning the joint Gaussian prior distribution on the observations we get,

$$f^* | \mathrm{X_*, X}, y \sim N(\bar{f}^*, V(f^*)) \tag{14}$$

The mean, $\bar{f}^*$ and variance, $\mathrm{V}(f^*)$ of the prediction at test points are given by:

$$\bar{f}^* = \mathrm{K(X_*, X)}\left[\mathrm{K(X_*, X)} + \sigma_n^2\mathrm{I}\right]^{-1} y \tag{15}$$

and

$$V(f^*) = \mathrm{K(X_*, X_*)} - \mathrm{K(X_*, X)}\left[\mathrm{K(X, X)} + \sigma_n^2\mathrm{I}\right]^{-1}\mathrm{K(X, X_*)} \tag{16}$$

For making prediction on test data, the GPR model requires the

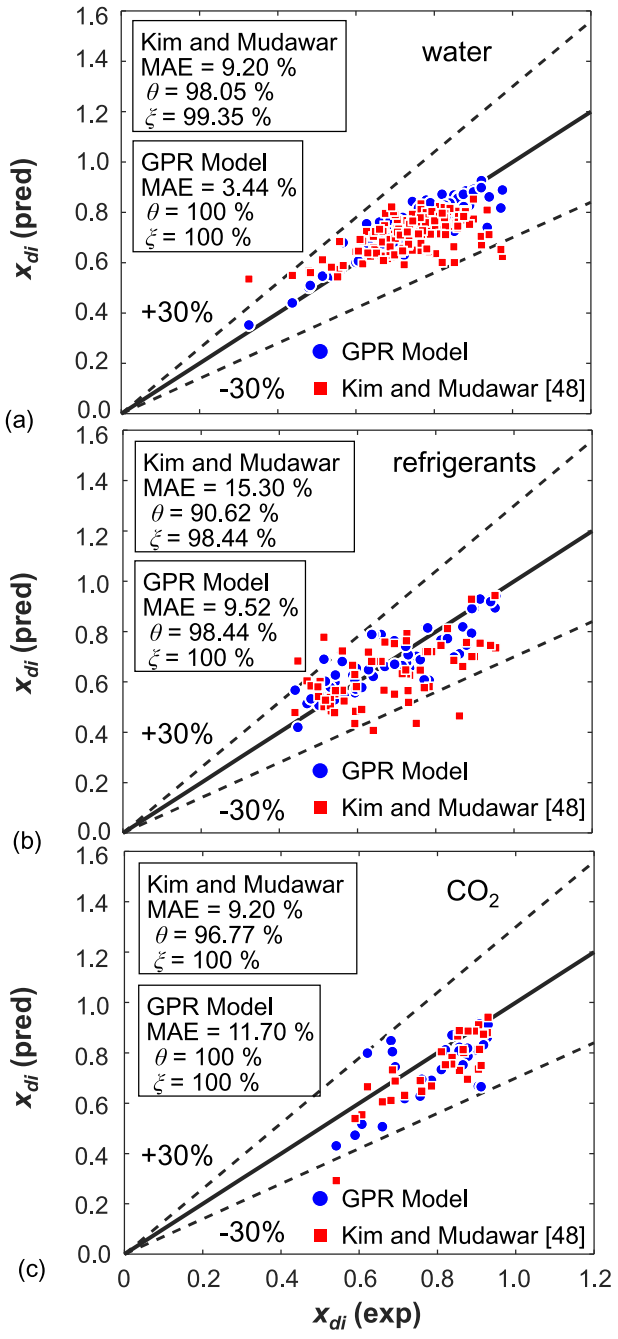

Fig. 7. Comparison of predictions from approved GPR model and universal correlation of Kim and Mudawar [48] for (a) water, (b) refrigerants and (c) CO_2.

knowledge of parameters, $\boldsymbol{\theta}$ and the noise variance, σ_n^2 which are estimated by maximizing the marginal log likelihood function given by:

$$\log p(y|\mathrm{X}) = -\frac{1}{2}y^T\left[\mathrm{K}(\mathrm{X},\mathrm{X})+\sigma_n^2\mathrm{I}\right]^{-1}y-\frac{1}{2}\log\left|\left[\mathrm{K}(\mathrm{X},\mathrm{X})+\sigma_n^2\mathrm{I}\right]^{-1}\right|-\frac{n}{2}\log 2\pi \tag{17}$$

The estimates of hyperparameters, θ and noise variance, σ_n^2 can be obtained as follows:

$$\widetilde{\theta},\widetilde{\sigma}_n^2 = \max_{\theta,\ \sigma_n^2}\log p(y|\mathrm{X}) \tag{18}$$

4. Results and discussion

In the present study, the GPR models were developed using MATLAB [83] running on an Intel Core i7 processor, 16 GB RAM and a clock speed of 2.90 GHz in serial processing mode. Quasi – newton method using trust – region, and symmetric rank – 1 based approximation to the hessian was used to perform minimization of the negative marginal log likelihood function. The GPR model was invoked using 'fitrgp' function available in 'Statistics and Machine Learning Toolbox' in MATLAB [83]. The input parameters were liquid – only weber number (We_{fo}), reduced pressure (P_R), boiling number (Bo), heated to frictional perimeter ratio (P_H/P_F), capillary number (Ca) and density ratio (ρ_g/ρ_f). The response variable was dryout incipience quality, x_{di}. The consolidated database of 997 points from 26 sources was partitioned randomly with 75% for training the GPR model and 25% for testing the prediction accuracy of the model. The accuracy of the approved GPR models on the training and testing sets was assessed using mean absolute error (MAE) similar to Kim and Mudawar [48], which is defined as:

$$\mathrm{MAE} = \frac{1}{n}\sum\frac{\left|x_{di,pred}-x_{di,\exp}\right|}{x_{di,\exp}}\times 100\,\% \tag{19}$$

where 'n' is the number of data points in training and testing sets, respectively. Also, the percentage of predictions within ±30% and ± 50% of the data are presented using parameters, θ and ξ, respectively.

As a preliminary step, a systematic investigation was carried out to select the best covariance function for the given input – output data. Six – different types of covariance functions, namely exponential, squared exponential, ARD exponential, ARD squared exponential, rational quadratic and ARD rational quadratic were tested. Fig. 4 shows a typical plot of minimization of the negative marginal log likelihood function with number of iterations for the ARD rational quadratic kernel. The relevant hyperparameters for each covariance function were determined from optimization as shown in Table 2. For ARD covariance functions, the characteristic length scales are listed for each input in the following order: We_{fo}, P_R, Bo, P_H/P_F, Ca and ρ_g/ρ_f. Fig. 5 shows the comparison of predicted and experimental dryout incipience quality for the entire 997 points consolidated database for the chosen covariance functions. A perfect regression line (solid black line) where the predicted response is equal to the true response, and ±30% error bands (dashed black lines) are also drawn for interpretation of model prediction accuracy. It can be seen that exponential, squared exponential and rational quadratic covariance functions showed significant and uneven scatter of test points around the line with high levels of under – and over – predictions. However, the discrepancy between the predicted and experimental results is significantly reduced with the use of ARD exponential, ARD squared exponential and ARD rational quadratic functions with points scattered roughly close and symmetric around the regression line indicating small prediction errors. Also, a very small number of points lying outside the ±30% error band. The superior performance of ARD class of covariance functions can be attributed to different characteristic length scales for each input variables compared to a constant length scale for non – ARD covariance functions. The MAE and θ were found to be 6.42%, 8.95%, 6.03% and 99.30%, 96.28%, 99.80% for ARD exponential, ARD squared exponential and ARD rational quadratic, respectively for the test data. The corresponding values of MAE and θ for the training data were 0.28%, 8.01%, 0.21% and 100%, 95.72%, 100%, respectively for the above ARD covariance functions. Therefore, the GPR model with ARD rational quadratic covariance function showed the best overall performance among all the tested cases, and therefore, will be selected as the final approved GPR model for further analysis.

A detailed comparison between approved GPR model and universal correlation proposed by Kim and Mudawar [48] in the prediction of dryout incipience quality using the full database (997 points) is shown in Fig. 6. For the present GPR model, the predictions on the test data are scattered very close to the regression line, which means the model has

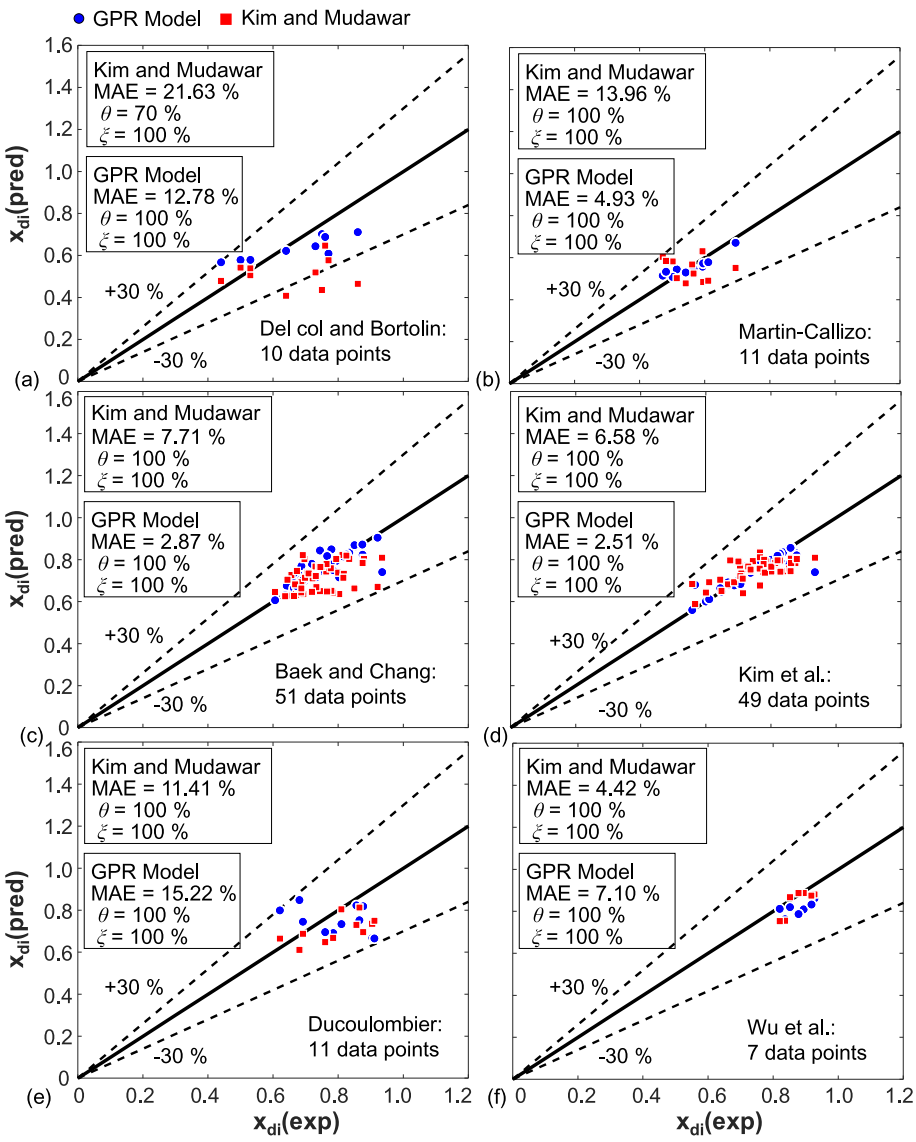

Fig. 8. Comparison of predictions from approved GPR model and universal correlation of Kim and Mudawar [48] on test data points from selected individual databases (a) Del Col and Bortolin [70], (b) Martin – Callizo [51], (c) Baek and Chang [58], (d) Kim et al. [60], (e) Ducoulombier [39] and (b) Wu et al. [53].

small errors and a good generalization ability. On the other hand, the predictions from the universal correlation showed slightly higher amount of error with 6.4 % of data points falling outside the ± 30 % error bands. Overall, the approved GPR model showed a superior prediction accuracy with MAE of 6.03 % and θ of 99.80 % compared to the universal correlation of Kim and Mudawar [48] that has MAE of 12.50 % and θ values of 93.60 %.

The prediction accuracy of the approved GPR model on the test data is further examined to study the effect of different working fluids i.e. refrigerants, water, CO_2, and compared with the universal correlation of Kim and Mudawar [48] as shown in Fig. 7. The results show that the present GPR model showed the better prediction results for water and refrigerants having lower MAE values of 3.44 % and 9.52 %, respectively, compared with 9.20 % and 15.30 % obtained by using the universal correlation of Kim and Mudawar[48]. A slight increase in MAE values, with 11.70 % for GPR model and 9.21 % for Kim and Mudawar [48], was observed for CO_2 which can be attributed to the low sample size of training data for CO_2 dryout incipience database for the GPR model compared with Kim and Mudawar [48]. In fact, only 75 % of the database was available for training the GPR model. Therefore, it is expected that the prediction accuracy of GPR model on CO_2 database can be improved if more training data is provided, particularly in regions of low dryout incipience qualities where there are high chances of under – and over – predictions as shown in Fig. 7. A similar trend is observed for predictions from universal correlation [48], but with relatively lower intensity of under – and over – predictions. This will also help to increase the overall accuracy of the GPR model for the entire consolidated database. Also, the percentage data predicted within ± 30 % error band is be 100 %, 98.44 %, 100 % for water, refrigerants, CO_2, respectively for the GPR model which is promising in terms of variance of the predictions.

Fig. 8 shows the predictions on the test data using the approved GPR model and the universal correlation of Kim and Mudawar [48] for some selected individual databases. The corresponding MAE on individual databases is shown in Fig. 9. The choice of individual databases was made to cover different working fluids i.e. water, refrigerants and CO_2 with appreciable sample sizes. Baek and Chang [58] and Kim et al. [60] based on water showed test data scattered very close to the regression line, and they have low MAE of 2.86 % and 2.51 %, respectively. Similarly, Martin – Callizo [51], which contains data for three different refrigerants, R134a, R22, and R245fa, showed all test points lying very close to the regression line, except for one outlier as shown in Fig. 8,

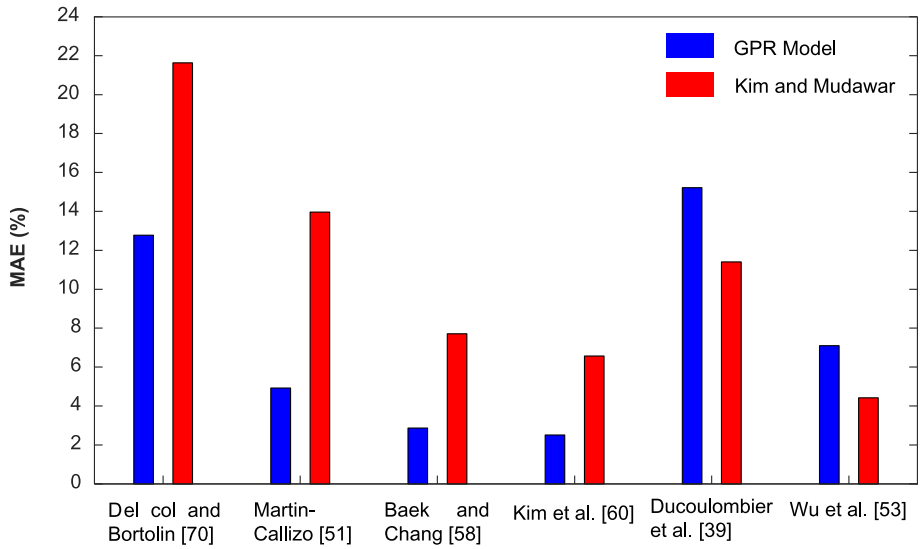

Fig. 9. Comparison of MAE evaluated on test points from selected individual databases using GPR model and universal correlation of Kim and Mudawar [48].

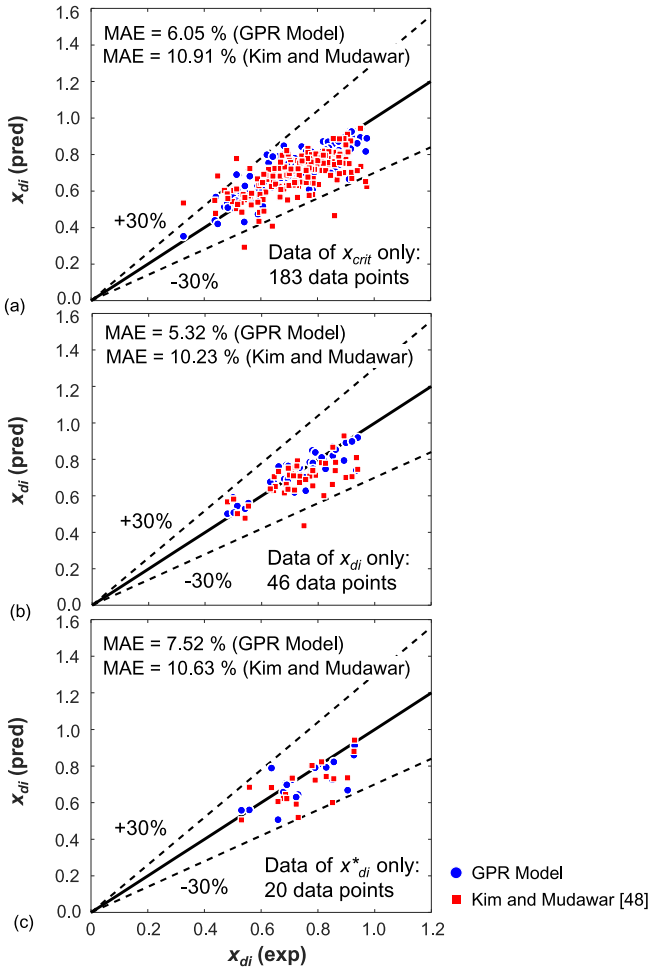

Fig. 10. Predictions from approved GPR model and universal correlation of Kim and Mudawar [48] for (a) x_{crit}, (b) x_{di} and (c) x^*_{di}.

with a MAE of 4.93 %. However, the data points were relatively more scattered for Del Col and Bortolin [70] which is also developed by only three refrigerants, R134a, R245fa and R32, with a MAE of 12.78 %, and over – predictions in low quality dryout and under – predictions in high quality dryout regions.

The GPR model predictions on the test data for three types of individual databases, based on x_{crit}, x_{di}, and, x^*_{di}, are shown in Fig. 10. The model showed the best results for dryout incipience quality, x_{di} followed by dryout completion quality, x_{crit} and dryout incipience quality, x^*_{di} databases with MAE values of 5.32 %, 6.05 % and 7.52 %, respectively. It can be concluded that the individual predictions are quite consistent, and with high accuracy. Also, the GPR model predictions were observed to be superior compared with the universal correlation of Kim and Mudawar [48] which predicted a nearly constant MAE value of approximately 10.50 % for all the three types of individual databases.

An exercise was carried out to check the generalization ability of GPR models for datasets outside its training set. The numerical experiment was carried by training on one of the three types of individual databases based on, x_{crit}, x_{di}, and, x^*_{di}, and predicting on the remaining two. But, to check the prediction on the training database it was partitioned randomly with 75% for training and 25% for testing. Fig. 11 shows the GPR model predictions for individual databases based on, x_{crit}, x_{di}, and, x^*_{di}, respectively. The GPR models showed good generalization ability on test sets sampled from individual databases based on, x_{crit}, x_{di}, and x^*_{di}, with low MAE values of 4.02 %, 7.51 % and 5.63 %, respectively, as shown in Fig. 11(a), (e), and (i). Therefore, provided that the training and test data comes from the same sample, GPR models can learn in a very efficient manner even with small datasets. Thus, GPR models can be a promising data efficient machine learning technique when obtaining large dataset can be either expensive or challenging as in experimental studies. For the database of dryout completion quality, x_{crit}, the GPR model showed a relatively poor prediction performance on excluded datasets based on x_{di} and x^*_{di}. A close examination reveals that the working fluid in the training set of water is completely different for the excluded datasets of refrigerants and CO_2, and therefore, without any history of working fluid in the training set, the GPR model was not able to perform well resulting in increase in MAE for the excluded datasets. Another important observation was the limited range of operation of dimensionless numbers for dryout completion quality, x_{crit}, database, therefore, rendering many test points from excluded dataset as outliers due to which the MAE was found to increase significantly. A similar trend was observed for the remaining individual databases based on x_{di} and x^*_{di} as depicted in Fig. 11 (d)(f) and (g)(h), respectively. Both databases predicted the dryout completion quality, x_{crit} with low MAE, 14.12 % for x_{di} and 16.13 % for x^*_{di}, due to the wide range of operation of dimensionless numbers covered leading to high diversity in the training

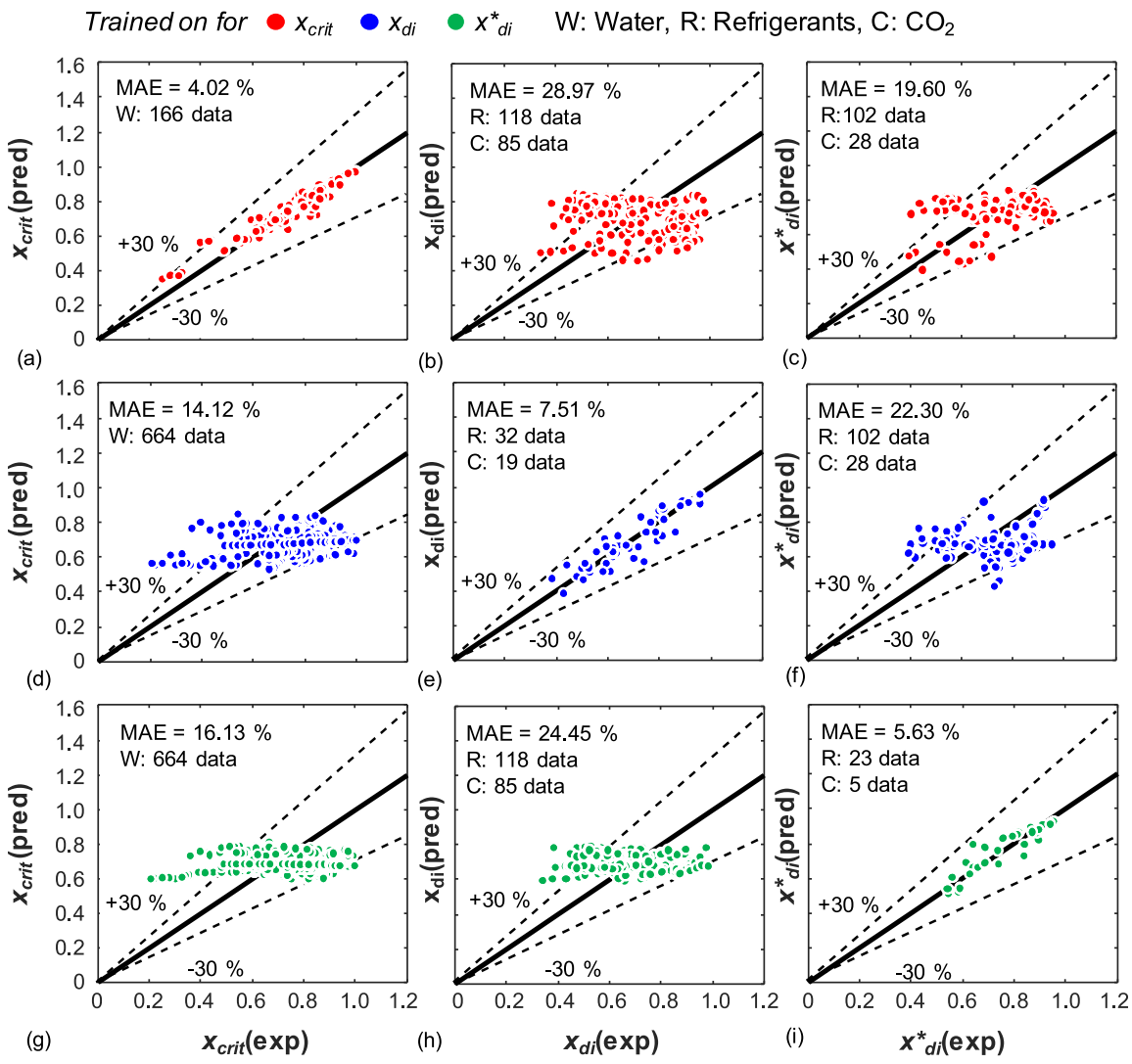

	Water(W)	Refrigerants(R)	CO_2
x_{crit}	664	0	0
x_{di}	0	118	85
x^*_{di}	0	102	28

Fig. 11. Predictions on test points using GPR model trained on for (a)(b)(c) x_{crit}, (d)(e)(f)x_{di} and (g)(h)(i) x^*_{di}.

set, and therefore better learning. On the other hand, both predicted individual excluded databases with high MAE. The individual databases based on x_{di} and x^*_{di} comprise of 203 and 130 data points, out of which the refrigerants – CO_2 pairs were 118 – 85 and 102 – 28, respectively. When the GPR model was trained on databases based on x_{di}, the training set has fewer data points than the test set, excluded database, using refrigerant as working fluid, and consequently, it did not generalize well on the test set leading to high MAE. This behavior is typical of any machine learning model. However, for the GPR model trained on databases based on x^*_{di}, the training set has significantly small number of data points using CO_2 as working fluid, and therefore, showed predictive poor performance on CO_2 test points in the excluded dataset leading to high MAE. Overall, the databases based on x_{di} showed the best overall performance on excluded datasets with lowest MAE of 15.46 % followed by x^*_{di} and x_{crit} those are showing 18.08 % and 25.31 % of MAE for excluded datasets, respectively.

Feature analysis is performed to evaluate the relative importance of each input feature on the dryout incipience quality, x_{di}. Permutation feature importance (PFI) algorithm [84] measures the discrepancy in the prediction error by randomly permuting a particular feature values in the data, thus breaking the relationship between the feature and the true output. A feature importance (FI) parameter is defined to measure the relative importance of each input feature; more important features generally have higher FI values. In the present study, the FI_i ($i = 1,2,\cdots,6$) for each feature is defined as the difference between original MAE (without random permutation) and permuted MAE_i (with random

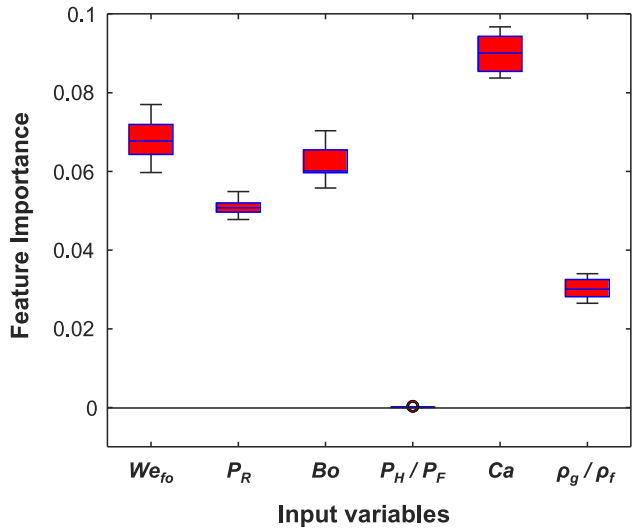

Fig. 12. Permutation feature importance (PFI) analysis of the input variables using approved GPR model.

permutation for each $i = 1, 2, \cdots, 6$) on the test data. Since the permutation was random, the PFI algorithm was run 10 times to eliminate any bias to randomness. Box plots are used to present the results of this analysis as shown in Fig. 12. The dimensionless parameters, capillary number, *Ca* and weber number We_{fo} showed highest impact on predictive performance of the GPR model followed by boiling number, *Bo*, reduced pressure, P_R, density ratio, ρ_g/ρ_f and heated to frictional perimeter ratio, P_H/P_F. In fact, a GPR model developed by excluding the least significant features, ρ_g/ρ_f and P_H/P_F resulted in a very small change in original MAE (from 6.03% to 6.41%).

Four dimensionless numbers, We_{fo},P_R,*Bo* and *Ca*, are able to describe the complex physics related to partial liquid film dryout and intermittent dryout. They are estimated to have a greater impact on the prediction results, having higher FI values compared to the other two, P_H/P_F and ρ_g/ρ_f. We_{fo} and *Ca* can explain the dryout incipience by partial liquid film breakage, which is induced by interfacial instability known as Kelvin-Helmholtz instability. The unstable interface condition is established when the liquid flow inertia and corresponding drag force exerting on the interface dominate over the surface tension, as they are related to imbalance and stabilizing force, respectively. When the interface becomes unstable and the troughs of the wavy interface touch the heated surface, the incipience dryout by partial liquid film breakage occurs. For the incipience of intermittent dryout, P_R and *Bo* can address the phenomenon as they are related to the liquid film evaporation rate. When the liquid film under periodic flow conditions is completely evaporated before the next flow surge period starts, intermittent dryout is triggered. The boiling number, *Bo*, represents the phase change rate, while the reduced pressure, P_R, determines the latent heat of evaporation, h_{fg}, which is related to the film evaporation rate.

5. Conclusions

A systematic study to develop an efficient GPR model to predict the dryout incipience quality for saturated flow boiling in mini/micro – channels has been performed in the present study. A consolidated database of 997 points from 26 sources was used to develop the GPR model which includes 13 different working fluids over a wide range of operating conditions: hydraulic diameter (0.51 – 6.0 mm), mass velocities (29 – 2303 kg/ m^2 s), liquid – only Reynolds number (125 – 53,770), boiling number (0.31 – 44.3 $\times$ 10^{-4}), and reduced pressure (0.005 – 0.78). Dimensionless variables, We_{fo}, P_R, *Bo*, P_H/P_F, *Ca* and ρ_g/ρ_f were passed as inputs to the GPR model, and dryout incipience quality was chosen as the output for learning. The consolidated database of 997 points from 26 sources was divided into training and test (75 % – 25 %) sets. Using training data, different types of covariance functions were tested, and as a result the ARD rational quadratic covariance function was selected based on the predictive performance on the test data. The superior performance can be attributed to different characteristic length scales for each input variables. The GPR model showed a very good accuracy with significantly low MAE of 6.03 %, and 99.80 % of data falling within the ±30% error band. A comparison with a popular universal correlation of Kim and Mudawar [48] showed a superior prediction ability of GPR model on the overall test data, and even individual test sets collected based on different working fluids i.e. refrigerants, water, CO_2 and selected individual databases. To check the extrapolation ability of GPR models, three different datasets grouped on the basis of identification of dryout incipience quality were generated. A GPR model was trained on one dataset at a time, and used to predict the excluded datasets. Results indicate a robust and good prediction ability of GPR models on reduced dataset (self), but a poor prediction ability on excluded sets due to the nature of working fluids in individual datasets, and the ranges of dimensionless parameters covered in the training samples. Even when the training samples are low, but a sufficient ranges of dimensionless parameters are included, the performance of GPR model was found to improve demonstrating data efficient behavior of GPR models. Finally, a feature importance analysis reveals the importance of each dimensionless parameter in descending order, *Ca*, We_{fo}, *Bo*, P_R, ρ_g/ρ_f and P_H/P_F. Future research aims to improve the robustness and prediction accuracy of the GPR model through strategic selection of important features from all relevant dimensionless parameters affecting the dryout incipience quality for saturated flow boiling in mini/micro – channels.

CRediT authorship contribution statement

Arshad Afzal: Investigation, Software, Data curation, Methodology, Formal Analysis, Writing – original draft. **Seunghyun Lee:** Conceptualization, Supervision, Writing – original draft, Writing – review & editing. **Sung-Min Kim:** Data curation, Writing – review & editing. **Issam Mudawar:** Writing – review & editing.

Declaration of competing interest

The authors declare that they have no known competing financial interests or personal relationships that could have appeared to influence the work reported in this paper.

Data availability

Data will be made available on request.

Acknowledgement

The authors are grateful for financial support from the National Research Foundation of Korea (NRF) grant funded by the Ministry of Science and ICT (MSIT) of Korea government (NRF-RS-2023-00280898) and acknowledge the support of the National Aeronautics and Space Administration (NASA) under grant no. 80NSSC22K0328.

References

[1] I. Mudawar, Assessment of high-heat-flux thermal management schemes, IEEE Trans. Compon. Packag. Technol. 24 (2001) 122–141.
[2] I. Mudawar, Two-phase micro-channel heat sinks: theory, applications and limitations, J. Electron. Packag. Trans. ASME. 133 (2011) 041002.
[3] J.G. Collier, J.R. Thome, Convective Boiling and Condensation, 3rd Ed., Oxford University Press, 1994.
[4] W. Qu, I. Mudawar, Thermal design methodology for high-heat-flux single-phase and two-phase micro-channel heat sinks, Proc. I-THERM 2002, San Diego, California, pp. 347-359.

[5] W. Qu, I. Mudawar, Experimental and numerical study of pressure drop and heat transfer in a single-phase micro-channel heat sink, Int. J. Heat Mass Transf. 45 (2002) 2549–2565.
[6] W. Qu, I. Mudawar, Flow boiling heat transfer in two-phase micro-channel heat sinks—I. Experimental investigation and assessment of correlation methods, Int. J. Heat Mass Transf. 46 (2003) 2755–2771.
[7] W. Qu, I. Mudawar, Measurement and prediction of pressure drop in two-phase micro-channel heat sinks, Int. J. Heat Mass Transf. 46 (2003) 2737–2753.
[8] J. Lee, I. Mudawar, Two-phase flow in high-heat flux micro-channel heat sink for refrigeration cooling applications: Part II. Heat transfer characteristics, Int. J. Heat Mass Transf. 48 (2005) 941–955.
[9] S. Lee, I. Mudawar, Investigation of flow boiling in large micro-channel heat exchangers in a refrigeration loop for space applications, Int. J. Heat Mass Transf. 97 (2016) 110–129.
[10] S. Lee, V.S. Devahdhanush, I. Mudawar, Investigation of subcooled and saturated boiling heat transfer mechanisms, instabilities, and transient flow regime maps for large length-to-diameter ratio micro-channel heat sinks, Int. J. Heat Mass Transf. 123 (2018) 172–191.
[11] R. van Erp, R. Soleimanzadeh, L. Nela, G. Kampitsis, E. Matioli, Co-designing electronics with microfluidics for more sustainable cooling, Nature 585 (2020) 211–216.
[12] M.K. Sung, I. Mudawar, Single-phase and two-phase heat transfer characteristics of low temperature hybrid micro-channel/micro-jet impingement cooling module, Int. J. Heat Mass Transf. 51 (2008) 3882–3895.
[13] T.J. LaClair, I. Mudawar, Thermal transients in a capillary evaporator prior to the initiation of boiling, Int. J. Heat Mass Transf. 43 (2000) 3937–3952.
[14] S. Mukherjee, I. Mudawar, Smart pumpless loop for micro-channel electronic cooling using flat and enhanced surfaces, IEEE Trans-CPMT: Compon. Packag. Tech. 26 (2003) 99–109.
[15] D.B. Tuckerman, R.F.W. Pease, High-performance heat sinking for VLSI, IEEE Electron Device Lett. 2 (1981) 126–129.
[16] P. Wang, P. McCluseky, A. Bar-Cohen, Two-phase liquid cooling for thermal management of IGBT power electronic module, J. Electron. Packag. 135 (2) (2013) 021001.
[17] S. Lee, I. Mudawar, Transient characteristics of flow boiling in large micro-channel heat exchangers, Int. J. Heat Mass Transf. 103 (2016) 186–202.
[18] Z. An, L. Jia, X. Li, Y. Ding, Experimental investigation on lithium-ion battery thermal management based on flow boiling in mini-channel, Appl. Therm. Eng. 117 (2017) 534–543.
[19] H. Tuo, P. Hrnjak, Flash gas bypass in mobile air conditioning system with R134a, Int. J. Refrig. 35 (7) (2012) 1869–1877.
[20] Q. Lu, Y. Liu, J. Deng, X. Luo, Z. Deng, Z. Mi, Review of interdisciplinary heat transfer enhancement technology for nuclear reactor, Ann. Nucl. Energy. 159 (2021) 108302.
[21] M.F. Wadel, Comparison of high aspect ratio cooling channel designs for a rocket combustion chamber, in: AIAA paper 1997-2913, 33rd AIAA/ASME/SAE/ASEE Joint Propulsion Conference, Jul. 1997.
[22] E.J. Choi, J.Y. Park, M.S. Kim, A comparison of temperature distribution in PEMFC with single-phase water cooling and two-phase HFE-7100 cooling methods by numerical study, Int. J. Hydrog. Energy 43 (29) (2018) 13406–13419.
[23] U. Soupremanien, S.L. Person, M. Favre-Marinet, Y. Bultel, Tools for designing the cooling system of a proton exchange membrane fuel cell, Appl. Therm. Eng. 40 (2012) 161–173.
[24] M.B. Bowers, I. Mudawar, Two-phase electronic cooling using mini-channel and micro-channel heat sinks - part 2. Flow rate and pressure drop constraints, J. Electron. Packag. 116 (1994) 298–305.
[25] W. Qu, I. Mudawar, Transport phenomena in two-phase micro-channel heat sinks, J. Electron. Packag. – Trans. ASME 126 (2004) 213–224.
[26] S. Lee, V.S. Devahdhanush, I. Mudawar, Frequency analysis of pressure oscillations in large length-to-diameter two-phase micro-channel heat sinks, Int. J. Heat Mass Transf. 116 (2018) 273–291.
[27] H.J. Lee, D.Y. Liu, S. Yao, Flow instability of evaporative micro-channels, Int. J. Heat Mass Transf. 53 (2010) 1740–1749.
[28] J. Lee, I. Mudawar, Critical heat flux for subcooled flow boiling in micro-channel heat sinks, Int. J. Heat Mass Transf. 52 (2009) 3341–3352.
[29] W. Qu, I. Mudawar, Measurement and correlation of critical heat flux in two-phase micro-channel heat sinks, Int. J. Heat Mass Transf. 47 (2004) 2045–2059.
[30] J. Lee, I. Mudawar, Fluid flow and heat transfer characteristics of low temperature two-phase micro-channel heat sinks – Part 2. Subcooled boiling pressure drop and heat transfer, Int. J. Heat Mass Transf. 51 (2008) 4327–4341.
[31] H. Jung, S. Lee, Mechanistic model to predict oscillating frequency of flow boiling in large length to diameter ratio micro-channel heat sinks, Int. J. Heat Mass Transf. 215 (15) (2023) 124473.
[32] I. Mudawar, M.B. Bowers, Ultra-high critical heat flux (CHF) for subcooled water flow boiling - I. CHF data and parametric effects for small diameter tubes, Int. J. Heat Mass Transf. 42 (1999) 1405–1428.
[33] G.F. Hewitt, A.H. Govan, Phenomenological modelling of non-equilibrium flows with phase change, Int. J. Heat Mass Transf. 33 (1990) 229–242.
[34] P.B. Whalley, P. Hutchinson, G.F. Hewitt, The calculation of critical heat flux in forced convection boiling, in: Proc. Fifth Int. Heat Transf, B6, Conf, Tokyo, Japan, Paper, 1974, pp. 290–294.
[35] S. Sugawara, Droplet deposition and entrainment modeling based on the three-fluid model, Nucl. Eng. Des. 122 (1990) 67–84.
[36] I. Kataoka, M. Ishii, A. Nakayama, Entrainment and deposition rates of droplets in annular two-phase flow, Int. J. Heat Mass Transf. 43 (2000) 1573–1589.
[37] R. Revellin, J. Thome, A theoretical model for the prediction of the critical heat flux in heated microchannels, Int. J. Heat Mass Transf. 51 (2008) 1216–1225.
[38] H. Mori, S. Yoshida, K. Ohishi, Y. Kakimoto, Dryout quality and post-dryout heat transfer coefficient in horizontal evaporator tubes, in: Eur. Therm. Sci. Conf., Germany, 2000, pp. 839-844.
[39] M. Ducoulombier, S. Colasson, J. Bonjour, P. Haberschill, Carbon dioxide flow boiling in a single microchannel – Part II: heat transfer, Exp. Therm. Fluid Sci. 35 (2011) 597–611.
[40] R. Mastrullo, A.W. Mauro, J.R. Thome, D. Toto, G.P. Vanoli, Flow pattern maps for convective boiling of CO2 and R410A in a horizontal smooth tube: experiments and new correlations analyzing the effect of the reduced pressure, Int. J. Heat Mass Transf. 55 (2012) 1519–1528.
[41] Z. Sun, CO_2 flow boiling heat transfer in horizontal tubes, Purdue University, West Lafayette, IN, 2001. Ph.D. Thesis.
[42] S.H. Yoon, E.S. Cho, Y.W. Hwang, M.S. Kim, K. Min, Y. Kim, Characteristics of evaporative heat transfer and pressure drop of carbon dioxide and correlation development, Int. J. Refrig. 27 (2004) 111–119.
[43] L. Wojtan, T. Ursenbacher, J.R. Thome, Investigation of flow boiling in horizontal tubes: Part I – a new diabatic two-phase flow pattern map, Int. J. Heat Mass Transf. 48 (2005) 2955–2969.
[44] L. Cheng, G. Ribatski, L. Wojtan, J.R. Thome, New flow boiling heat transfer model and flow pattern map for carbon dioxide evaporating inside horizontal tubes, Int. J. Heat Mass Transf. 49 (2006) 4082–4094.
[45] D. Del Col, F. Fantini, L. Rossetto, Dryout quality in a minichannel flow boiling, in: XXV UIT National Heat Transf. Conf., Italy, 2007, pp. 18–20.
[46] L. Cheng, G. Ribatski, J.M. Quibén, J.R. Thome, New prediction methods for CO2 evaporation inside tubes: part I – a two-phase flow pattern map and a flow pattern based phenomenological model for two-phase flow frictional pressure drops, Int. J. Heat Mass Transf. 51 (2008) 111–124.
[47] S. Jeong, D. Park, Evaporative heat transfer of CO_2 in a smooth and a micro-grooved miniature channel tube, Heat Transf. Eng. 30 (2009) 582–589.
[48] S.M. Kim, I. Mudawar, Universal approach to predicting saturated flow boiling heat transfer in mini / micro – channels – Part I. Dryout incipience quality, Int. J. Heat Mass Transf. 64 (2013) 1226–1238.
[49] R. Yun, Y. Kim, M.S. Kim, Convective boiling heat transfer characteristics of CO_2 in microchannels, Int. J. Heat Mass Transf. 48 (2005) 235–242.
[50] L. Wang, M. Chen, M. Groll, Flow boiling heat transfer characteristics of R134a in a horizontal mini tube, J. Chem. Eng. Data 54 (2009) 2638–2645.
[51] C. Martín-Callizo, Flow boiling heat transfer in single vertical channel of small diameter, Royal Institute of Technology, Sweden, 2010. Ph.D. Thesis.
[52] H.K. Oh, C.H. Son, Evaporation flow pattern and heat transfer of R-22 and R- 134a in small diameter tubes, Heat Mass Transf. 47 (2011) 703–717.
[53] J. Wu, T. Koettig, Ch. Franke, D. Helmer, T. Eisel, F. Haug, J. Bremer, Investigation of heat transfer and pressure drop of CO_2 two-phase flow in a horizontal minichannel, Int. J. Heat Mass Transf. 54 (2011) 2154–2162.
[54] M. Li, C. Dang, E. Hihara, Flow boiling heat transfer of HFO1234yf and R32 refrigerant mixtures in a smooth horizontal tube: part I. Experimental investigation, Int. J. Heat Mass Transf. 55 (2012) 3437–3446.
[55] R. Ali, B. Palm, Dryout characteristics during flow boiling of R134a in vertical circular minichannels, Int. J. Heat Mass Transf. 54 (2011) 2434–2445.
[56] K.M. Becker, Burnout measurements in vertical round tubes, effect of diameter, AE-TPM-RL-1260, Aktiebolaget Atomenergi, 1970.
[57] A.M. Lezzi, A. Niro, G.P. Beretta, Experimental data on CHF for forced convection water boiling in long horizontal capillary tubes, in: Proc. 10, Int. Heat Transf. Conf, vol. 7, UK, 1994, pp. 491–496.
[58] W.P. Baek, S.H. Chang, KAIST CHF data, Personal communication, Korea Advanced Institute of Science and Technology, Taejon, South Korea, 8, 1997.
[59] G.M. Roach Jr., S.I. Abdel-Kahlik, S.M. Ghiaasiaan, M.F. Dowling, S.M. Jeter, Low-flow critical heat flux in heated microchannels, Nucl. Sci. Eng. 131 (1999) 411–425.
[60] H.C. Kim, W.P. Baek, S.H. Chang, Critical heat flux of water in vertical round tubes at low pressure and low flow conditions, Nucl. Eng. Des. 199 (2000) 49–73.
[61] Y. Yang, Y. Fujita, Boiling heat transfer in rectangular channels of small gaps, Memoirs of the Faculty of Engineering, Kyushu University 62 (2002) 223–239.
[62] W. Yu, D.M. France, M.W. Wambsganss, J.R. Hull, Two-phase pressure drop, boiling heat transfer, and critical heat flux to water in a small-diameter horizontal tube, Int. J. Multiph. Flow 28 (2002) 927–941.
[63] S. Saitoh, H. Daiguji, E. Hihara, Effect of tube diameter on boiling heat transfer of R-134a in horizontal small-diameter tubes, Int. J. Heat Mass Transf. 48 (2005) 4973–4984.
[64] E. Hihara C. Dang Boiling heat transfer of carbon dioxide in horizontal tubes Proc. 2007 ASME–JSME Therm. Eng. Summer Heat Transf 2007 Conf., Canada, HT2007-32885 843 849.
[65] A. Greco, Convective boiling of pure and mixed refrigerants: an experimental study of the major parameters affecting heat transfer, Int. J. Heat Mass Transf. 51 (2008) 896–909.
[66] D. Shiferaw, Two-phase flow boiling in small- to micro-diameter tubes, Brunel University, UK, 2008. Ph.D. Thesis.
[67] H. Ohta, K. Inoue, M. Ando, K. Watanabe, Experimental investigation on observed scattering in heat transfer characteristics for flow boiling in a small diameter tube, Heat Transf. Eng. 30 (2009) 19–27.
[68] H.K. Oh, C.H. Son, Flow boiling heat transfer and pressure drop characteristics of CO in horizontal tube of 4.57-mm inner diameter, Appl. Therm. Eng. 31 (2011) 163–172.
[69] J.T. Oh, A.S. Pamitran, K.I. Choi, P. Hrnjak, Experimental investigation on twophase flow boiling heat transfer of five refrigerants in horizontal small tubes of

0.5, 1.5 and 3.0 mm inner diameters, Int. J. Heat Mass Transf. 54 (2011) 2080–2088.
[70] D. Del Col, S. Bortolin, Investigation of dryout during flow boiling in a single microchannel under non-uniform axial heat flux, Int. J. Therm. Sci. 57 (2012) 25–36.
[71] T.G. Karayiannis, M.M. Mahmoud, D.B.R. Kenning, A study of discrepancies in flow boiling results in small to micro diameter metallic tubes, Exp. Therm. Fluid Sci. 36 (2012) 126 142.
[72] C.B. Tibiriçá, G. Ribatski, J.R. Thome, Flow boiling characteristics for R1234ze(E) in 1.0 and 2.2 mm circular channels, ASME, J. Heat Transf. 134 (2012) 020906.
[73] A.M. Ghahdarijani, F. Hormozi, A.H. Asl, Convective heat transfer and pressure drop study on nanofluids in double-walled reactor by developing an optimal multilayer perceptron artificial neural network, Int. Commun. Heat Mass Transf. 84 (2017) 11–19.
[74] P. Naphon, T. Arisariyawong, Heat transfer analysis using artificial neural networks of the spirally fluted tubes, J. Res. Appl. Mech. Eng. 4 (2016) 135–147.
[75] Y. Qiu, D. Garg, L. Zhou, C.R. Kharangate, S.M. Kim, I. Mudawar, An artificial neural network model to predict mini / micro – channels saturated flow boiling heat transfer coefficient based on universal consolidated data, Int. J. Heat Mass Transf. 149 (2020) 119211.
[76] R. Pearce, P. Ireland, E. Romero, Thermal matching using Gaussian process regression, Proceedings Inst. Mech. Engineers, Part g: J. Aerospace Eng. 234 (6) (2020) 1172–1180.
[77] A. Afzal, K.-Y. Kim, Optimization of pulsatile flow and geometry for a convergent – divergent micromixer, Chem. Eng. J. 281 (2015) 134–143.
[78] S.M. Kim, A. Afzal, K.-Y. Kim, Optimization of a staggered jet-convex dimple array cooling system, Int. J. Therm. Sci. 99 (2016) 161–169.
[79] Y. Duan, C. Cooling, J.S. Ahn, C. Jackson, A. Flint, M.D. Eaton, M.J. Bluck, Using a Gaussian process regression inspired method to measure agreement between the experiment and CFD simulations, Int. J. Heat Fluid Flow 80 (2019) 108497.
[80] S.M. Kim, I. Mudawar, Universal approach to predicting two-phase frictional pressure drop for mini/micro-channel saturated flow boiling, Int. J. Heat Mass Transf. 58 (2013) 718–734.
[81] J.B. Copetti, M.H. Macagnan, F. Zinani, N.L.F. Kunsler, Flow boiling heat transfer and pressure drop of R-134a in a mini tube: an experimental investigation, Exp. Therm. Fluid Sci. 35 (2011) 636–644.
[82] C.E. Rasmussen, C.K.I. Williams, Gaussian processes for machine learning, MIT press, 2006.
[83] The MathWorks Inc., Statistics and Machine Learning Toolbox Documentation, Natick, Massachusetts: The MathWorks Inc. (2022).
[84] A. Fisher, C. Rudin, F. Dominici, All models are wrong, but many are useful: learning a variable's importance by studying an entire class of predictions models simultaneously, J. Mach. Learn. Res. 20 (177) (2019) 1–81.